ELSEVIER

Chemical Engineering Journal 100 (2004) 51–69

Chemical Engineering Journal

www.elsevier.com/locate/cej

The composition dependence of self and transport diffusivities from molecular dynamics simulations

David J. Keffer*, Parag Adhangale

Department of Chemical Engineering, University of Tennessee, 1512 Middle Drive, Knoxville, TN 37996-2200, USA

Received 28 June 2003; accepted 29 November 2003

Abstract

Using molecular dynamics (MD) simulations, we determine the composition dependence of the self-diffusivity and transport diffusivity of a methane/ethane mixture at high pressure. The transport diffusivity is generated from the self-diffusivities using the Darken equation. We perform a careful analysis of the molecular dynamics simulations and show that it is possible to reproduce the results in the microcanonical, canonical, and isobaric–isothermal ensembles. We demonstrate that in order to capture the sensitive dependence of the diffusivities on composition, it is necessary to run simulations with larger systems and for longer durations than is typical. We report the trends in the diffusivities as a function of composition, temperature, pressure, and density. We modify an existing empirical correlation, which when combined with a corresponding states chart, is capable of quantitatively reproducing the simulated diffusivity dependence on composition, temperature, pressure, and density. Finally, we quantify the effect that the choice of equation of state (EOS) used to evaluate the thermodynamic factor in the Darken equation has on the transport diffusivity.

Keywords: Isobaric–isothermal; Temperature; Pressure; Molecular dynamics; Darken equation; Self-diffusivity; Transport diffusivity

1. Introduction

The estimation of diffusivities using theoretical, experimental, and simulation approaches has been of practical interest for many decades. Kinetic theory can predict the self-diffusivity of pure (single-component) dilute gases quantitatively [1]. It can also predict the self-diffusivity of pure dense fluids quantitatively, given that values of the collision integral are available. Many empirical correlations to determine the self-diffusivity as a function of temperature, pressure, and molecular weight have also been developed [2,3]. Additionally, plots based on corresponding states, which are fitted to experimental and simulation data, can predict self-diffusivities of dense fluids semi-quantitatively [3]. However, for many systems there are no theories or correlations that can accurately predict the self-diffusivity. Frequently, the best and sometimes the only recourse is to turn to experiment. Typically in the determination of self-diffusivities, the experiments fall into two categories: laboratory experiments and computer simulations. We classify computer simulations as a type of experiment, since the only theoretical concepts that necessarily feed into the simulations are Newton's second law and the choice of a force field to describe molecular interactions.

Before we can continue our introduction, we must distinguish between self-diffusivities and transport diffusivities. We provide a qualitative description here and a mathematical definition later. A self-diffusivity is a measure of the mobility of fluid molecules in the absence of a driving force for diffusion, e.g. a composition gradient. Self-diffusivities arise due to the Brownian (random-walk) motion of the molecules. Self-diffusivities are defined for pure fluids as well as for each component in a mixture.

Transport diffusivities, also known as Fick or Fickian diffusivities, appear in Fick's law. They relate a mass or mole flux to a driving force, such as a gradient in the concentration of a particular species. Transport diffusivities are typically not defined for pure fluids. For a multicomponent fluid containing n_c components, the transport diffusivity is typically represented as an $n_c \times n_c$ matrix, although not all of the elements of this matrix are independent. Transformations of this matrix are possible, generally to an $(n_c - 1)\times(n_c - 1)$ matrix, where each element of the upper triangular component of the matrix is independent. Transport diffusivities arise due to gradients in the system.

When one chooses to evaluate Fick's law, one requires transport diffusivities rather than self-diffusivities. In

* Corresponding author. Tel.: +1-865-974-5322; fax: +1-865-974-7076.
E-mail address: dkeffer@utk.edu (D.J. Keffer).

1385-8947/$ – see front matter © 2004 Elsevier B.V. All rights reserved.
doi:10.1016/j.cej.2003.11.028

addition to self-diffusivities, kinetic theory can also predict transport diffusivities. It is easy to use kinetic theory to predict the transport diffusivities of low-pressure gases and substantially more difficult to predict them for dense fluids. Empirical correlations and corresponding-states plots, while intended for self-diffusivities of pure fluids, have also been modified to estimate transport diffusivities, at least for binary fluids. However, these modifications do not predict the transport diffusivity (or the self-diffusivity) as a function of the composition of the mixture. In other words, there is no dependence of the self-diffusivities and transport diffusivity on mole fractions.

In this work, we employ molecular dynamics (MD) simulations to estimate the self-diffusivities and transport-diffusivities of a high pressure binary mixture of methane and ethane. We specifically determine the composition dependence of the diffusivities. We describe how existing correlations and charts can be easily modified to give quantitative agreement with simulation.

In Section 2, we provide a review of the pertinent literature. In Section 3, we provide a detailed discussion of our simulation techniques, including our efforts to minimize statistical error. In Section 4, we present the results of our simulations. We also test the validity of the modified correlations, we have developed. Finally, in Section 5, we present our conclusions.

2. Background

2.1. Simulation

2.1.1. Self-diffusivities from simulation

It is a standard procedure to estimate self-diffusivities in pure components or mixtures using equilibrium molecular dynamics (EMD) simulations [4–6]. One can use either of two equivalent methods to obtain a self-diffusivity for each component in the mixture. The first method is to use Einstein's relation, which relates the mean square displacement to the observation time via

$$D_{\mathrm{self},\alpha} = \frac{1}{2d}\lim_{\tau\to\infty}\frac{1}{\tau}\langle[r_{\alpha,i}(t+\tau) - r_{\alpha,i}(t)]^2\rangle \tag{1}$$

where $D_{\mathrm{self},\alpha}$ is the self-diffusivity of component α, d the dimensionality of the system, τ the observation time, and $r_{\alpha,i}$ is the position of the ith molecule of component α. The brackets indicate an ensemble average over time, t, and over all molecules of component α. There is no ambiguity in defining the self-diffusivity. Moreover, there are no practical obstacles in the determination of a self-diffusivity from a molecular dynamics simulation, aside from the ubiquitous concerns that the simulation include a sufficient number of molecules and be of adequate duration so as to ensure acceptable statistical accuracy of the results.

A second method to determine the self-diffusivity is to use the velocity auto-correlation function in a Green–Kubo relation [4–6]

$$D_{\mathrm{self},\alpha} = \frac{1}{d}\int_0^\infty \langle v_{\alpha,i}(t+\tau)\cdot v_{\alpha,i}(t)\rangle \mathrm{d}\tau \tag{2}$$

where $v_{\alpha,i}$ is the velocity of the ith molecule of component α. Again, there is no practical impediment to implementation, except to be aware that this integral contains a long-time tail.

2.1.2. Transport diffusivities from simulation

There are several ways that one can measure the transport diffusivity of a mixture in an MD simulation. First, one can perform a non-equilibrium MD simulation. For example, Heffelfinger and van Swol [7] developed and used the dual control-volume grand-canonical molecular dynamics (DCV-GCMD) simulation to measure transport diffusivities [7]. Using this technique, one established a gradient in chemical potential. One measures the flux. One can then use Fick's law to back out the transport diffusivity. Maginn and Bell [8] used color field theory and non-equilibrium MD simulations to generate transport diffusivities. This method, although more efficient than DCV-GCMD, is still computationally expensive. Arya et. al. [9] have also compared equilibrium MD simulations, with external field non-equilibrium MD (EF-NEMD) and the DCV-GCMD simulations for consistency in transport coefficients and the computational expense. They report that both EMD and EF-NEMD are far more efficient than DCV-GCMD.

A second method to determine the transport diffusivity is to run equilibrium MD simulations, as described above, and to invoke the Darken equation [10]. The Darken equation can be written as

$$D_{\alpha\beta} = \left(\frac{\partial \ln a_\alpha}{\partial \ln x_\alpha}\right)_{T,p}(x_\alpha D_{\mathrm{self},\beta} + x_\beta D_{\mathrm{self},\alpha}) \tag{3}$$

where k_B is Boltzmann's constant, T temperature, a_α the activity of component α, and x_α is the mole fraction. Although the Darken equation was published in 1948 to describe diffusion in binary alloys, it has been widely used for a variety of systems in the subsequent half century. There are numerous approximations involved in the Darken equation and there exist decades of literature attempting to quantify the magnitude of error resulting from those approximations [11,12]. Carman summarizes his findings, "... the Darken type of equation and probably any equation based upon a simple premise cannot be expected to give a highly accurate correlation with experimental data in most systems." [11]. Nevertheless, the Darken equation is still widely used in both experimental and simulated systems to compute transport diffusivities from self-diffusivities [13]. The appeal of the Darken equation is that it requires only self-diffusivities, which can be obtained in an unambiguous manner and with some statistical significance from a single equilibrium MD simulation.

A third method of obtaining the transport diffusivities is to adopt the formalism of linear irreversible thermodynamics,

in which one can relate transport diffusivities to phenomenological coefficients. These phenomenological coefficients in turn can be obtained from equilibrium MD simulations [8,14,15]. Again the phenomenological coefficients can be obtained from equivalent Green–Kubo or Einstein-like relations. The disadvantage with this method lies in the fact that the phenomenological coefficients display a far greater susceptibility to statistical noise than do the self-diffusivities. Therefore, in order to obtain a statistically reliable diffusivity from the phenomenological coefficients, one must average the results of many simulations. Previous researchers have used an average over 10–14 [15].

Sometimes the transport diffusivity is called the "mutual diffusion coefficient" [16,17]. This mutual diffusion coefficient is a transport diffusivity for a binary system relative to a local center of volume frame of reference. It effectively is using linear irreversible thermodynamics to obtain the transport diffusivity. As such, numerous simulations are required to obtain a reasonable standard deviation. Jolly and Bearman averaged 27 estimates [16].

Apart from these methods listed above for obtaining the transport diffusivity, there are other techniques. For example, Ali et al. [18] employed mode coupling theory to estimate transport diffusivities of binary Lennard–Jones systems [18]. The full advantage of this approach has not yet been explored.

Of these methods, the Darken equation is the least rigorous, but has the advantage that it requires the least computation time because self-diffusivities take less simulation effort to compute than transport diffusivities. The reason lies in the fact that each molecule contributes independent information to the self-diffusivity at every time step, effectively providing N data points to which the self-diffusivity will be fit. However, the transport diffusivities examine system properties, like center-of-mass position, which provide only one piece of information per time step.

In the Darken equation, one must still calculate the thermodynamic factor. There are a variety of ways to do this. Here we discuss two methods. First, if one has an equation of state (EOS) that describes the simulated fluid relatively well, then one can simply use the equation of state to evaluate the activity and the necessary partial derivative of the activity, which is the thermodynamic factor in the Darken equation. If one chooses this approach, then one does not require additional simulation time and maintains the advantage of the Darken equation.

Alternatively, one can use molecular simulations to determine the thermodynamic factor. For example, there are methods to determine the chemical potential of a molecular-level simulation. One common method is called Widom's particle insertion method [4,19]. In this method, one attempts to regularly insert particles into the simulation. Depending upon the ease with which the particles are accepted, one can determine the chemical potential. This method only works well for gases. As the fluid becomes more dense, the acceptance probability is so low that the method typically becomes computationally impractical.

To obtain the derivative of the chemical potential with respect to mole fraction, as needed for the thermodynamic factor in Darken's equation, one could then use a centered-finite difference formula. If the system of interest was at T, p, and mole fraction, x_α, then one would simulate the system at T, p, and mole fraction, $x_\alpha + \Delta x$ and at T, p, and mole fraction, $x_\alpha - \Delta x$. Widom's particle insertion method would be performed in all three simulations. Clearly, these simulations would be most easily accomplished in the isobaric–isothermal ensemble. Other researchers used grand canonical Monte Carlo (GCMC) simulations to determine the thermodynamic factor [15].

In this work, we are simulating bulk fluids. We will demonstrate that the Lennard–Jones equation of state predicts the simulated thermodynamic properties well [20]. We will use the Lennard–Jones equation of state to determine the thermodynamic factor.

2.2. Theory, empirical correlations and corresponding states plots

In this section, we make no attempt to review the rich and lengthy history of the theoretical estimation of diffusivities. Instead, we cite several specific theories and empirical correlations that we will test, modify, and compare with our simulation data.

We begin with kinetic theory of a dilute gas. The mean molecular speed of component α is

$$\bar{u}_\alpha = \frac{\sqrt{8k_B T}}{\sqrt{\pi m_\alpha}} \tag{4}$$

where m_α is the mass of 1 mol of component α. The mean free path, λ,

$$\lambda = \frac{1}{\sqrt{2}\pi\sigma_\alpha^2 n} \tag{5}$$

where n is the number density and σ_α is the collision diameter of a molecule of component α. When we compare to simulations, σ_α is the Lennard–Jones size parameter. Using these definitions, the familiar expression from kinetic theory for the self-diffusivity of a pure fluid of component α is

$$D_{\text{self},\alpha} = \frac{1}{3}\bar{u}_\alpha\lambda = \frac{2}{3}\frac{1}{\pi\sigma_\alpha^2 n}\frac{\sqrt{kB}}{\sqrt{\pi m_\alpha}} \tag{6}$$

We have a basic prediction of the functional relationship of the self-diffusivity on density, temperature, molecular size, and molecular weight. Eq. (6) rigorously applies only to single-component ideal gases.

Eq. (6) has no composition dependence. Thus, it cannot be used to predict the self-diffusivity of each component in a binary mixture. However, one can modify Eq. (6) to predict the self-diffusivities of components in a mixture by using the mean velocity of each component in Eq. (4). We can

build in composition dependence by using a mean diameter defined as

$$\bar{\sigma} = \sum_{\alpha=1}^{n_c} x_\alpha \sigma_\alpha \tag{7}$$

in Eq. (5), where n_c is the number of components in the mixture. Making these substitutions in Eq. (6) yields

$$D_{\text{self},\alpha}(\mathfrak{x}) = \frac{1}{3}\bar{u}_\alpha \lambda = \frac{2}{3}\frac{1}{\pi\bar{\sigma}^2 n}\frac{\sqrt{kB}}{\sqrt{\pi m_\alpha}} \quad \text{for } \alpha = 1 \text{ to } n_c \tag{8}$$

Using Eq. (8), we can calculate distinct self-diffusivities for all components in the mixture. We can expect that this equation will only apply at low pressure. We will compare our simulation results to Eq. (8).

A second approach to predicting the self-diffusivity of components in a mixture is to modify an existing corresponding states relationship. One can use a corresponding-states chart to obtain a value of $(cD_{\text{self},\alpha})_r$ where this product of the concentration and self-diffusivity is reduced by the same product at the critical point, $(cD_{\text{self},\alpha})_c$

$$(cD_{\text{self},\alpha})_r = \frac{(cD_{\text{self},\alpha})}{(cD_{\text{self},\alpha})_c} \tag{9}$$

Charts are available and require only a reduced temperature and pressure [3]. If one does not know the value of the self-diffusivity at the critical point, one can use an empirical formula to estimate it, such as [3]

$$(cD_{\text{self},\alpha\alpha^*})_c = 2.96 \times 10^{-6}\left(\frac{1}{M_\alpha}+\frac{1}{M_{\alpha^*}}\right)^{1/2}\frac{p_{c\alpha}^{2/3}}{T_{c\alpha}^{1/6}} \tag{10}$$

where the units for this correlation are concentration [mol/cm^3]; self-diffusivity [cm^2/s]; critical pressure, $p_{c\alpha}$, [atm]; critical temperature, $T_{c\alpha}$, [K]; and molecular weight, M_α, [g/mol]. The α^* component appears because this equation was originally developed for isotope diffusion. If we are examining self-diffusion in a simulation, then both the α and α^* component have the same mass. The problems with Eq. (10) are that (i) it does not apply to components in mixtures and (ii) it does not have any composition dependence. We can modify Eq. (10) to remedy these shortcomings by using mixing rules to estimate the critical pressure and temperature. The mixing rule employed in this work is

$$\bar{T}_c = \sum_{\alpha=1}^{n_c}\sum_{\beta=1}^{n_c} x_\alpha x_\beta \sqrt{T_{c,\alpha}T_{c,\beta}} \tag{11}$$

We used the same mixing rule for the critical pressure. A modified version of Eq. (10) can be written

$$(cD_{\text{self},\alpha})_c = 2.96 \times 10^{-6}\left(\frac{2}{M_\alpha}\right)^{1/2}\frac{\bar{p}_c^{2/3}}{\bar{T}_c^{1/6}} \quad \text{for } \alpha = 1 \text{ to } n_c \tag{12}$$

Eq. (12) can be used to generate distinct self-diffusivities at the critical point for each component in the mixture. Moreover, those critical self-diffusivities will be functions of composition. Using Eq. (12) in conjunction with a corresponding states chart, we are able to predict the self-diffusivities of methane and ethane for the states we simulated in this work. Note, that the mean critical properties are used not only in Eq. (12) but also to calculate the reduced temperature and pressure required to use the corresponding-states plot. We expect that Eq. (12) will deliver more accurate predictions than Eq. (8) because the corresponding states chart is based on laboratory and simulation data.

We can now attempt to predict the transport diffusivity. We will make three different approximations. The first is to modify an empiricism based on both kinetic theory and corresponding states, which originally had the form, [21]

$$\frac{pD_{\text{tran}}}{(p_{c,\alpha}p_{c,\beta})^{1/3}(T_{c,\alpha}T_{c,\beta})^{5/12}(1/M_\alpha+1/M_\beta)^{1/2}} = 2.745\times10^{-4}\left(\frac{T}{\sqrt{T_{c,\alpha}T_{c,\beta}}}\right)^{1.823} \tag{13}$$

where this equation requires the same units as Eq. (10). The shortcoming of Eq. (13) is that it has no composition dependence. We modified this empiricism in a manner that was analogous to transforming Eqs. (10)–(12). In short, we replaced the critical values with mean critical values that were functions of composition.

A second prediction of the transport diffusivity is to take an expression completely analogous to Eq. (10) and use a corresponding states chart. Typically, this expression is written

$$(cD_{\text{tran}})_c = 2.96\times10^{-6}\left(\frac{1}{M_\alpha}+\frac{1}{M_\beta}\right)^{1/2}\frac{\sqrt{p_{c,\alpha}p_{c,\beta}^{2/3}}}{\sqrt{T_{c,\alpha}T_{c,\beta}^{1/6}}} \tag{14}$$

Again, Eq. (14) contains no dependence on the mole fractions. We replace the critical pressures and temperature with mean values that are functions of composition, as given in Eq. (11) to obtain a prediction that is a function of composition.

$$(cD_{\text{tran}})_c = 2.96\times10^{-6}\left(\frac{1}{M_\alpha}+\frac{1}{M_\beta}\right)^{1/2}\frac{\bar{p}_c^{2/3}}{\bar{T}_c^{1/6}} \tag{15}$$

A third prediction of the transport diffusivity is to use the self-diffusivities, predicted by Eq. (8) or a corresponding-states chart and Eq. (12), in the Darken equation, Eq. (3). We will compare all three of these predictions to our simulation results.

3. Simulation

3.1. General notes

The molecular dynamics simulations performed in this work were conducted using a homemade molecular

dynamics code in FORTRAN 90. In a molecular dynamics simulation, there are three sets of parameters that need to be defined. The first set of parameters defines the thermodynamic state and includes for a canonical ensemble the temperature, T, the simulation volume, V, and the number of molecules of each chemical species in the simulation, N_i. The second set of parameters defines the identity of each chemical species. In our simulations, we used the Lennard–Jones potential to model intermolecular interactions. Therefore, we can completely identify the ith chemical species with three parameters: σ_i, the collision diameter, ε_i, the energetic well depth, and M_i, the molecular weight. One should also include in this second set of parameters, the long distance cut-off for the intermolecular interaction, r_{cut}, since it effectively determines the long-range mean-field correction to the internal energy and pressure. The third set of parameters defines the numerical procedure used to integrate the classical equations of motion. The parameters include the type of algorithm, the size of the time step, and the number of time steps used during the equilibration stage and the data production stage of the simulation. Knowing these three sets of parameters completely defines the simulation. It is true that other parameters exist, such as (i) the interval for updating a neighbor list, if a neighbor list is used to increase the computational efficiency of the simulation, or (ii) the size of the cell, if a linked-cell structure is used to increase efficiency, or for that matter (iii) the interval at which sampling is performed to obtain thermodynamic and transport properties. However, these additional parameters, if chosen properly, do not affect the result of the simulation and therefore are in a sense auxiliary parameters.

In the following sections, we provide the additional details of the simulations in various ensembles.

Table 1
Simulation parameters

Thermodynamic parameters	
Total number of molecules	10000
Temperature (K)	350
Molar volume (Å^3/mol)	392.62
Chemical identity properties	
Intermolecular potential	Lennard Jones
σ_{CH_4} (Å)	3.822
$\sigma_{C_2H_6}$ (Å)	4.418
ε_{CH_4} (K)	137
$\varepsilon_{C_2H_6}$ (K)	230
M_{CH_4} (g/mol)	16.042
$M_{C_2H_6}$ (g/mol)	30.068
Long-range cut-off distance (Å)	15
Numerical integration parameters	
Integration algorithm	Gear fifth-order predictor corrector[fn]
Time step (fs)	2
Number of equilibration steps	100000
Number of data production steps	1000000
Auxiliary parameters	
Sampling interval for thermodynamic properties (fs)	2
Sampling interval for transport properties (fs)	2000
Temperature-controlling frequency (fs^{-1})	10^{-5}
Pressure-controlling frequency (fs^{-1})	10^{-5}
Diffusivity parameters	
Minimum elapsed time (fs)	500000
Maximum elapsed time (fs)	1000000

3.2. Microcanonical ensemble

The microcanonical ensemble is a very satisfying ensemble for molecular dynamics simulations because one can monitor the conservation of momentum and the conservation of energy and thus reassure oneself that all goes well in the simulation. We assured ourselves that energy was conserved by checking that the standard deviation of the total energy of the system, U, was much smaller than the standard deviation of either the kinetic, KE, or potential, PE, energies (which should be equal).

$$\sigma_U << \sigma_{KE} \approx \sigma_{PE} \tag{16}$$

Energy conservation is of course a function of step size. In practice, we saw that for our simulations, with the base parameters as defined in Table 1, that the standard deviation of the total energy is, on average, a factor of 63 (±22) times smaller than the average of the standard deviations of the kinetic and potential energies. The conservation of momentum was typically good to 14 significant figures. The reason that the momentum is conserved to many more significant figures than the energy is that, even when the numerical method used to integrate the equations of motion results in a slightly erroneous force, that same erroneous force is applied to both molecules (opposite in sign for one molecule) comprising the pair in the pair-wise Lennard–Jones interaction, and thus momentum is conserved within machine truncation error.

The microcanonical ensemble has the disadvantage that one has to specify the total energy, when one typically would rather specify the temperature (or equivalently the kinetic energy). Traditionally, one can get around this by using velocity scaling during the equilibration stage of the simulation. At the end of equilibration, one should have a system at the average potential energy and the exact set temperature. Using then the microcanonical ensemble (i.e. ceasing velocity scaling) for the data production run, should maintain that same temperature on a time-averaged basis. However, in practice, there is a flaw in this procedure. The flaw lies in the fact that during the canonical equilibration, the potential energy fluctuates about an average. If one stops the equilibration stage arbitrarily, the potential energy is not at the average value. Instead, it is fluctuating somewhere around the average value. The consequence of this is that, shifting to the microcanonical ensemble at this point, fixes the system to a state that does not correspond to the average potential energy. If the last value of the potential energy during equilibration was higher than the average, then it will drop

during the microcanonical production stage and the kinetic energy will commensurately rise, increasing the temperature beyond the set point. The reverse case, causing a decrease in temperature, is equally likely.

We developed a technique to avoid this problem by equilibrating in three stages when simulating in the microcanonical ensemble. In the first stage, we perform the normal equilibration for 0.2 ns. In the second stage of equilibration, we are already equilibrated, but we continue the canonical simulation for 0.1 ns and gather data on the average potential energy. The sole purpose of the second stage of equilibration is to determine the average potential energy. We do not use the average potential energy from the first stage of equilibration because that contains data during the transition to equilibrium. The third and final stage of equilibration lasts only a few thousand femtoseconds. We monitor the instantaneous value of the potential energy until it matches within an acceptable tolerance the average value from the second stage of equilibration. When the two values do match, we begin the microcanonical data production stage of the simulation immediately. This assures that the total energy of the microcanonical simulation corresponds to the sum of the true kinetic and average potential energies of the system. This eliminates the temperature shift in moving from the canonical equilibration to microcanonical data production stage. This technique was used in all microcanonical simulations presented in this work.

3.3. Canonical ensemble

In this work, we will compare diffusivities obtained for the same system in the microcanonical and canonical ensembles. The temperature was maintained constant in the canonical ensemble using the Hoover formulation of the Nosé thermostat, henceforth referred to as the Nosé–Hoover thermostat [22,23]. This thermostat was used in preference to other popular techniques for simulating in the canonical ensemble, such as (i) velocity scaling [5]; (ii) the original Nosé thermostat [24]; and Berendsen's thermostat [25] for several reasons. First, there is no significant computational advantage to one thermostat over another; all require nominal CPU resources relative to the force evaluation. Second, the Nosé and Nosé–Hoover thermostats generate trajectories in the canonical ensemble. It has been proven that they do so uniquely [23]. Third, the Nosé–Hoover thermostat is a more eloquent and less inconvenient formulation of the Nosé thermostat because the time-scaling issue disappears, meaning that all time steps in the MD simulation are of equal size when using the Nosé–Hoover thermostat. We employ the Nosé–Hoover thermostat for all canonical simulations in this work because of its rigor and convenience. Moreover, we follow the formalism of Melchionna et al. [23] which present the Nosé–Hoover thermostat in a clear and elegant manner in which it has an obvious analog in the isobaric–isothermal ensemble, discussed shortly.

The Nosé–Hoover thermostat requires one parameter, which controls the period (but not the amplitude) of the temperature fluctuations around the mean. In Hoover's formalism, this parameter, sometimes called the thermal inertial parameter has units of mass times length squared. This parameter, Q, also scales with the number of molecules in the simulation. We prefer the more intuitive reformulation of Melchionna et al. [23] which presents the single parameter as a frequency, ν_T, with units of inverse time, where the subscript T indicates that it is the temperature-controlling frequency (in the isobaric–isothermal ensemble, there will also be a pressure-controlling frequency). Our base case numerical value of the parameter is $\nu_T = 10^{-5}\,\mathrm{fs}^{-1}$. We provide justification for this value below.

3.4. Isothermal-isobaric ensemble

In this work, we will compare diffusivities obtained for the same system in the microcanonical and the isothermal-isobaric ensembles. The temperature was maintained constant in the isothermal-isobaric ensemble using the same formulation of the Nosé–Hoover thermostat described above. The pressure was maintained constant in the isothermal-isobaric ensemble using the analogous barostat of Melchionna et al. [23]. This barostat provides trajectories in the isobaric–isothermal ensemble, in contrast to other formulations of the barostat [26].

The Melchionna barostat requires one parameter, which controls the period (but not the amplitude) of the pressure fluctuations around the mean. This parameter is a frequency, ν_P, with units of inverse time, where the subscript P indicates that it is the pressure-controlling frequency. Our base case numerical value of the parameter is $\nu_P = 10^{-5}\,\mathrm{fs}^{-1}$.

3.5. Self-diffusivity

We obtain a self-diffusivity from the simulations via Einstein's relation. However, we modify the traditional form, as is given in Eq. (1). The problem with Eq. (1) is that it yields a self-diffusivity, which is a function of any center-of-mass motion of the simulated system. It is obvious that this is the case since, if the system were undergoing a uniform motion with a non-zero velocity, the displacement due to the mass-averaged velocity would contribute to the mean square displacement.

Indeed, center-of-mass motion in a simulation can be caused by an external field, in which case the center-of-mass motion is characterized by the mass-average velocity. Alternatively, the random center-of-mass motion can also be caused by thermostats. For example, if one simulates in the canonical ensemble, one must use a thermostat to control the temperature. Thermostats not only violate conservation of energy, but in multicomponent systems violate conservation of momentum as well. So even if a system begins with zero net momentum, the center of mass can still shift due to a thermostat. The drift with the Nose–Hoover thermostat

depends upon the magnitude of the temperature-controlling frequency. Simulations in the isobaric–isothermal ensemble can have center-of-mass drift due to both the temperature and pressure controllers.

It is desirable to have a diffusivity relative to a mass-averaged velocity, or in the case of a simulation, the center-of-mass motion, because the diffusivity must be calculated in the same frame of reference in which it is to be used. For example, if one writes the flux equation,

$$\underline{j}_\alpha = -\rho D_{\alpha\beta} \nabla w_\alpha \tag{17}$$

where $\underline{j}_\alpha$ is the diffusive mass flux of component α relative to the mass-average velocity, ρ the mass density, and w_α is the mass fraction of component α, then the transport diffusivity must have been calculated relative to the center-of-mass motion. Since we will relate the self-diffusivity to the transport diffusivity via the Darken equation, we must have the self-diffusivities calculated relative to the same frame of reference. It can be proven that the diffusivity in Eq. (17) is the same diffusivity that appears in an alternate expression of Fick's law

$$\underline{J}^*_\alpha = -cD_{\alpha\beta} \nabla x_\alpha \tag{18}$$

where $\underline{J}^*_\alpha$ is the diffusive molar flux of component α relative to the molar-average velocity, c the molar concentration, and x_α is the mole fraction of component α.

If we use Eq. (1) to calculate the self-diffusivity, and the center-of-mass of the simulation drifts for any of the reasons given above, then we can still use that diffusivity in a flux equation like Eq. (17), but now the mass flux contains that same center-of-mass motion and is no longer purely diffusive. If we did not record the center-of-mass motion, then we can't evaluate the flux relative to the laboratory frame of reference.

To ensure that we measure a diffusivity relative to the center-of-mass motion, we rewrite Eq. (1) as

$$D_{\text{self},\alpha} = \frac{1}{6} \lim_{\tau\to\infty} \frac{1}{\tau} \langle [(\underline{r}_{\alpha,i}(t+\tau) - \underline{r}_{\text{com}}(t+\tau)) - (\underline{r}_{\alpha,i}(t) - \underline{r}_{\text{com}}(t))]^2 \rangle \tag{19}$$

This mean square displacement is now relative to the net center-of-mass motion that took place from time t to time $t+\tau$. In this work, we calculate the diffusivity for all simulations using both Eqs. (1) and (19).

Regardless of our choice of frame of reference, using the Einstein relation requires that one perform a linear least squares regression of the mean square displacement (MSD) as a function of time. Because Einstein's relation is true only at long times, the intercept of this fit is non-zero. The intercept does not have any useful physical meaning, but it cannot be assumed to be zero. We record positions every 2 ps during the simulation lasting 2 ns. It is possible therefore to generate MSD for elapsed times of 2–2000 ps. However, Einstein's relation only holds in the long time limit. Therefore, we do not want to regress to data before that limit. Furthermore, we desire statistically accurate diffusivities. There is only one data point per molecule for the MSD at an elapsed time of 2000 ps. However, there are 501 data points per molecule for the MSD at an elapsed time of 1000 ps because we can examine an elapsed time from $t = 0$ to $t = 1000$, $t = 2$ to $t = 1002$ ... until $t = 1000$ to $t = 2000$ ps. Therefore, our upper limit on elapsed time is bounded by statistical accuracy. In general, we have found the following rule to be useful. We set the lower limit of the elapsed time to one quarter of the simulation duration. We set the upper limit of the elapsed time to one-half of the simulation duration. We perform our regression only between these limits. It is an arbitrary set of limits, but it is one that satisfies both the requirement that we be in the long-time limit and that we have good statistics, provided of course, that the total duration of the simulation is sufficient to capture the temporal fluctuations in the dynamics of the system. Moreover, these limits have the advantage that they have now been unambiguously defined. We use these limits for all regressions yielding the self-diffusivity in this work.

The regression is performed for each of the three dimensions independently. Since, the fluid is isotropic, we report the average diffusivity. The standard deviation (the errors bars in the plots of the diffusivity) is determined from the three values obtained for each dimension.

In Table 1, we list the default parameters used for the simulations in this work. All simulations use these parameters unless explicitly specified otherwise.

3.6. Transport diffusivity

As noted above, there are many different ways to formulate the transport diffusivity, depending upon the choice of frame of reference and diffusive driving force (e.g. gradient of mole fraction or concentration of α, or chemical potential of α, etc.) Since we intend to compare our results to the predictions of kinetic theory, empirical correlations, and corresponding-states charts, we need to make sure that the transport diffusivities that we generate are relative to the same frame of reference and apply to the same flux law. The transport diffusivities described above are intended to be used in a flux equation of the form given in Eq. (17) [3].

In this work, we compute our transport diffusivities using the Darken equation, Eq. (3). It is true that this method of estimation contains approximations not present in the other methods described. However, because the other methods are subject to greater statistical noise, in this paper we limit ourselves to the Darken equation. We intend to investigate the discrepancies between the various approaches of computing transport diffusivities for this system.

We use the Lennard–Jones equation of state to compute the thermodynamic factor in the Darken equation. In order to obtain the mixture parameters for the Lennard–Jones equation of state, we used Eq. (7) for the mixing rule of the collision diameter and Eq. (11) for the mixing rule of

the energetic well depth. We will show that this EOS does an excellent job of predicting the thermodynamic properties that the simulation does generate, such as pressure. Finally, we use both Eqs. (1) and (19) to obtain the self-diffusivities, so that we can compare the two equations.

4. Results and discussion

4.1. Diffusivity sensitivity to simulation parameters

In this work, we anticipate that the trends in the self- and transport-diffusivities relative to thermodynamic state variables that we are attempting to observe and establish are sensitive to noise in the simulation results. Therefore, the first task in our study was to verify that we could generate reproducible trends in the data. To this end, we performed simulations in the microcanonical ensemble varying both the number of molecules in the system and the duration of the production stage of the simulation. Our base simulation included a total of 10^4 molecules (regardless of composition) and 10^6 production time steps. These values are unusually large for the simulation of a homogeneous fluid. However, we felt that we needed at least 10^3 molecules of each species present. Thus, with 10^4 molecules, we could simulate mixtures with mole fractions from 0.1 to 0.9. The results of these simulations are shown in Fig. 1. Also shown on this plot are linear fits of the self-diffusivity of the form:

$$D_{\text{self},\alpha} = c^{(0)}_{\text{self},\alpha} + c^{(1)}_{\text{self},\alpha} x_{\text{Me}} \tag{20}$$

The transport diffusivity is fit with a quadratic polynomial of the form:

$$D_{\text{tran}} = c^{(0)}_{\text{tran}} + c^{(1)}_{\text{tran}} x_{\text{Me}} + c^{(2)}_{\text{tran}} x^2_{\text{Me}} \tag{21}$$

The purpose in fitting Eq. (20) to the self-diffusivity and Eq. (21) to the transport diffusivity is not to suggest some functional dependence of the diffusivities on composition. On the contrary, our motives in performing this fitting are statistical in nature. In order to compare our different simulations across the entire range of composition, it is necessary to create parameters that incorporate information across the range and can be rigorously statistically characterized, in terms of mean and variance. The coefficients of Eq. (20) and (21) fit this criterion. The coefficients were obtained using linear least squares regression to the simulation data and are reported in Table 2. The errors reported in Table 2 represent one standard deviation, as generated by the regression analysis.

In Fig. 1, we find that the self-diffusivities of methane and ethane increase nearly linearly with an increase in the mole fraction of methane. The error bars in Fig. 1 and all subsequent figures represent one standard deviation. It is important to realize in Fig. 1 that what is being held constant is (i) the total number of molecules; (ii) the temperature; and (iii)

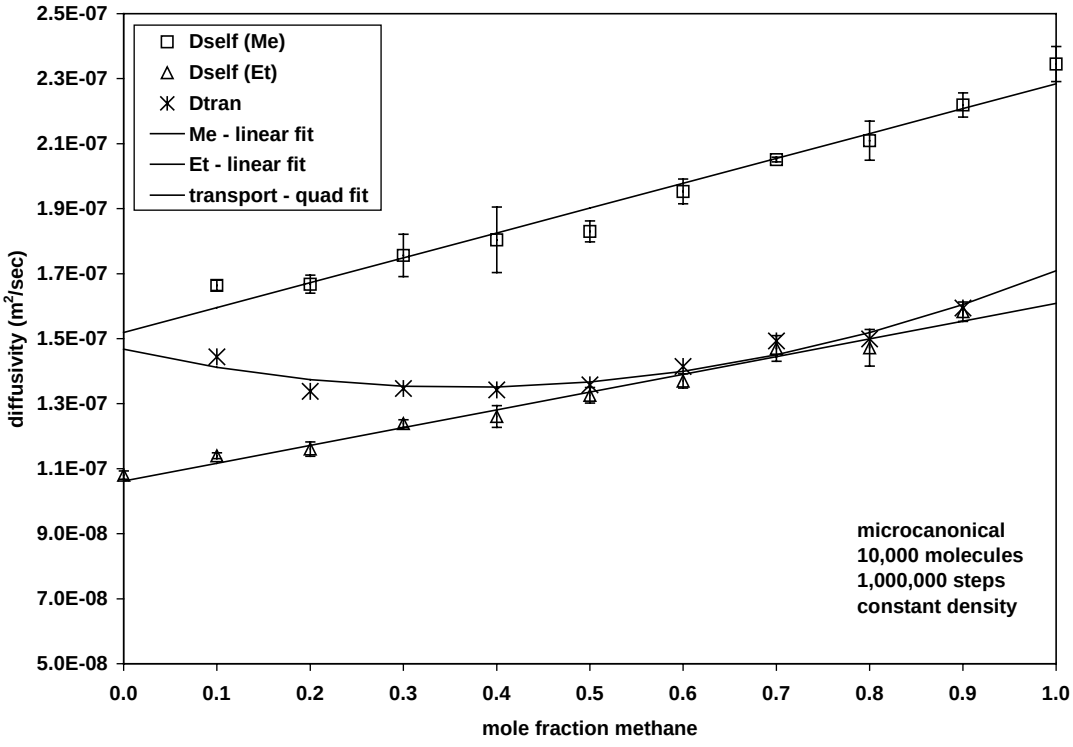

Fig. 1. Self-diffusivities and transport diffusivity for mixtures of methane and ethane as a function of composition at a temperature of 350 K and a density of 2.547×10^{-3} molecules/Å^3. These results come from the microcanonical ensemble using base case parameters of 10^4 molecules and 10^6 production steps. The polynomial fits are provided for statistical purposes only.

the system volume. Thus, in Fig. 1, the molar density is constant at all points. The value of the density is 2.5472×10^{-3} molecules/Å^3. The mass density and the pressure change at each simulation point.

We also fit the self-diffusivity to a first-order polynomial and the transport diffusivity to a second-order polynomial. We remind the reader that the linear functional form of the self-diffusivity on mole fraction and the quadratic functional form of the transport diffusivity on mole fraction is not substantiated by any molecular-level physics. On the contrary, we assume this form by inspection of the curves. That said, the self-diffusivities are remarkably linear with mole fraction. The coefficients and the measures of fit of the regressions (MOF) are reported in Table 2. The MOF of the regression on the self-diffusivities of methane and ethane are respectively 0.969 and 0.978. The MOF on the regression of the transport diffusivity is 0.921. We do not claim that the dependence of transport diffusivity on mole fraction is quadratic, but the high MOF indicates that the data follows some smooth curve that is relatively well approximated by a parabola. An increase in noise in the data would diminish these fits because it would diminish the smoothness of the curve.

The pressure for this set of simulations is shown in Fig. 2. We expect the pressure to increase with an increase in methane mole fraction based on the fact that the value of the energetic interaction parameters for ethane is greater than that for methane. Ethane has a much stronger attraction to other molecules, effectively reducing the pressure in the system, when temperature and molar density are held constant.

Four equations of state—the ideal gas, van der Waals, Peng–Robinson, and the Lennard–Jones equation of state—are also plotted in Fig. 2 for reference purposes. In order to implement the van der Waals and Peng–Robinson equations of state, we required some physical properties, including critical properties. The values that we used are given in Table 3 [27]. With these properties, we can calculate all of the parameters in the van der Waals and Peng–Robinson equations of state [27]. We point out now and will take advantage of the fact later that the Lennard–Jones equation of state models a high-pressure binary mixture of methane and ethane extremely well. The average relative error of the Lennard–Jones equation of state with respect to the simulation values is 0.13%. By comparison the average errors of the ideal gas, van der Waals, and Peng–Robinson EOS are 29.7, 4.1, and 5.2% respectively. The ideal gas EOS is qualitatively wrong because, of course, the pressure of an ideal gas has no composition dependence.

By comparing, Figs. 1 and 2, one can see that the self-diffusivities increase with increasing pressure, when the molar volume and temperature are held constant. This may be counter-intuitive and will be discussed in Section 4.3.

In Figs. 1 and 2, we simulated the system in the microcanonical ensemble. As such the temperature was not fixed. As described above, we can set the total energy so as to have a kinetic energy that corresponds to a desired temperature. In the eleven simulations shown in Figs. 1 and 2, the

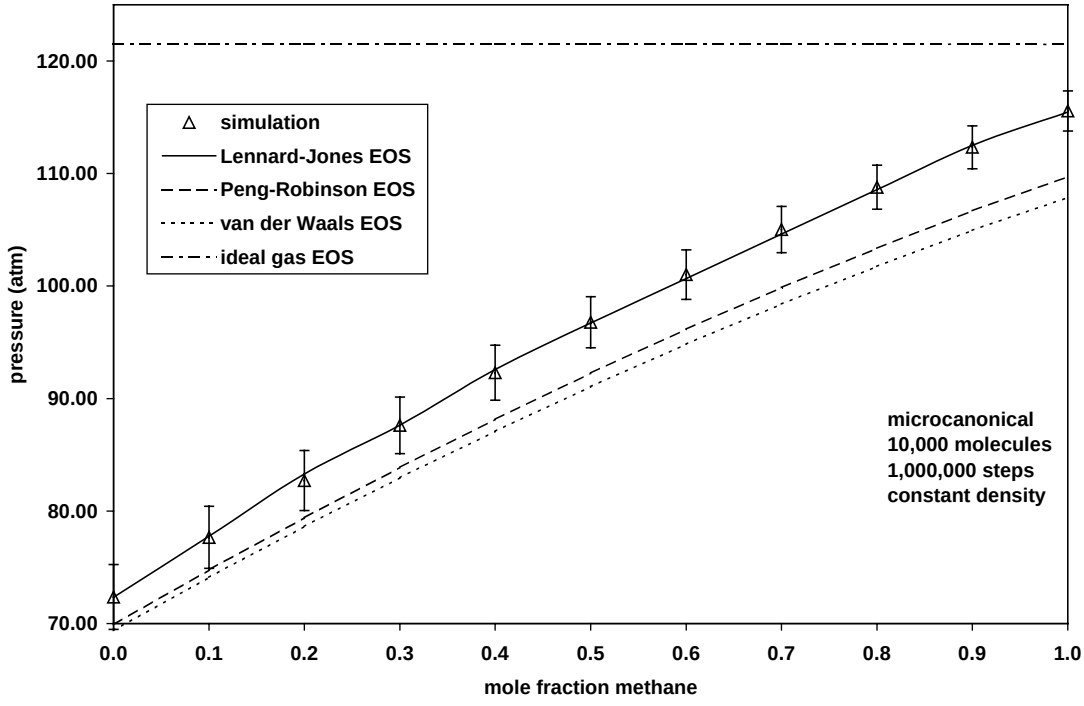

Fig. 2. Pressure for mixtures of methane and ethane as a function of composition at a temperature of 350 K and a density of 2.547×10^{-3} molecules/Å^3. These results come from the microcanonical ensemble for the base-case simulation, the small system, and the short simulation. The equations of state are provided for comparison purposes.

Table 2
Regression coefficients and uncertainties

Ensemble	Number of molecules	Number of time steps	Component	Constant coefficient (m^2/s)	Linear coefficient (m^2/s)	Quadratic coefficient (m^2/s)	MOF
Microcanonical	10^4	10^6	Methane	$15.19 \times 10^{-8} \pm 0.30 \times 10^{-8}$	$7.65 \times 10^{-8} \pm 0.48 \times 10^{-8}$	–	0.969
			Ethane	$10.62 \times 10^{-8} \pm 0.17 \times 10^{-8}$	$5.47 \times 10^{-8} \pm 0.31 \times 10^{-8}$	–	0.978
			Transport	$14.68 \times 10^{-8} \pm 0.37 \times 10^{-8}$	$8.88 \times 10^{-8} \pm 1.66 \times 10^{-8}$	$-6.46 \times 10^{-8} \pm 1.71 \times 10^{-8}$	0.921
			Methane	$15.53 \times 10^{-8} \pm 0.65 \times 10^{-8}$	$6.50 \times 10^{-8} \pm 1.05 \times 10^{-8}$	–	0.828
Microcanonical	10^3	10^6	Ethane	$10.76 \times 10^{-8} \pm 0.23 \times 10^{-8}$	$4.27 \times 10^{-8} \pm 0.41 \times 10^{-8}$	–	0.940
			Transport	$14.37 \times 10^{-8} \pm 0.88 \times 10^{-8}$	$5.44 \times 10^{-8} \pm 3.96 \times 10^{-8}$	$-4.33 \times 10^{-8} \pm 4.06 \times 10^{-8}$	0.362
			Methane	$14.82 \times 10^{-8} \pm 0.24 \times 10^{-8}$	$7.99 \times 10^{-8} \pm 0.38 \times 10^{-8}$	–	0.982
Microcanonical	10^4	10^5	Ethane	$10.54 \times 10^{-8} \pm 0.14 \times 10^{-8}$	$5.42 \times 10^{-8} \pm 0.25 \times 10^{-8}$	–	0.986
			Transport	$14.69 \times 10^{-8} \pm 0.38 \times 10^{-8}$	$9.22 \times 10^{-8} \pm 1.70 \times 10^{-8}$	$-6.77 \times 10^{-8} \pm 1.74 \times 10^{-8}$	0.889
			Methane	$14.92 \times 10^{-8} \pm 0.18 \times 10^{-8}$	$7.93 \times 10^{-8} \pm 0.29 \times 10^{-8}$	–	0.989
Canonical	10^4	10^6	Ethane	$10.41 \times 10^{-8} \pm 0.09 \times 10^{-8}$	$5.83 \times 10^{-8} \pm 0.17 \times 10^{-8}$	–	0.994
			Transport	$14.07 \times 10^{-8} \pm 0.26 \times 10^{-8}$	$7.31 \times 10^{-8} \pm 1.18 \times 10^{-8}$	$-4.40 \times 10^{-8} \pm 1.41 \times 10^{-8}$	0.963
			Methane	$15.28 \times 10^{-8} \pm 0.30 \times 10^{-8}$	$7.55 \times 10^{-8} \pm 0.49 \times 10^{-8}$	–	0.984
Isobaric–isothermal	10^4	10^6	Ethane	$10.42 \times 10^{-8} \pm 0.15 \times 10^{-8}$	$5.67 \times 10^{-8} \pm 0.27 \times 10^{-8}$	–	0.994
			Transport	$14.79 \times 10^{-8} \pm 0.44 \times 10^{-8}$	$9.74 \times 10^{-8} \pm 1.99 \times 10^{-8}$	$-7.26 \times 10^{-8} \pm 0.97 \times 10^{-8}$	0.900

Table 3
Equation of state parameters [27]

Parameter	Methane	Ethane
Critical temperature (K)	190.6	305.3
Critical pressure (bar)	46.1	49.0
Binary interaction parameter	−0.003	−0.003
Acentric factor	0.008	0.098

average temperature is 350.16 K with an average standard deviation of 0.88 K. The maximum average simulation temperature observed was 351.15 K at a methane mole fraction of 0.2. The minimum average simulation temperature observed was 349.72 K at a methane mole fraction of 0.7. This slight fluctuation in the temperature should contribute very little to noise in the diffusivities.

In order to ensure that we had a sufficient system size and simulation duration, we next conducted a second set of eleven simulations with only 10^3 molecules run for the full 10^6 time steps (the small system) as well as a third set of simulations with 10^4 molecules run for only 10^5 time steps (the short simulation). Both of these sets of simulations gave average values of the thermodynamic properties (e.g. pressure, internal energy, constant-volume heat capacity) in excellent agreement with our base case simulation set. If we were to choose as our basis for judgment a thermodynamic variable such as the pressure, it would seem that there is no significant difference between the results of the base case, small system, and short simulation.

In Fig. 3, we plot the diffusivities obtained from the small system (10^3 molecules run for the full 10^6 time steps). The noise in the data is substantially greater than in the base case. This noise is particularly evident at a mole fraction of 10% methane, where we have only 100 methane molecules. In order to compare the results of the small and large simulation systems in a statistically reliable manner, we can examine the coefficients of the linear fits to the self-diffusivities and the quadratic fits to the transport diffusivity. We find that for both self-diffusivities and the transport diffusivity, the MOF decreases with a decrease in system size. In fact the transport diffusivity shrinks from 0.921 to 0.362. Moreover, the standard deviations of the regression coefficients grow as we decrease system size. Consider, for example, the quadratic coefficient for the transport diffusivity regression. The standard deviation of the quadratic coefficient increases from 26.5% of the average coefficient value for the large system to 93.8% of the average value for the small system. Therefore, we conclude that, while the thermodynamic properties, such as the pressure, were reliably duplicated by the small system, we cannot establish statistically significant trends in the diffusivity with only 1000 molecules in the system.

Diffusivities were also obtained from the short simulation (10^4 molecules run for 10^5 time steps). The plot of these diffusivities as a function of the mixture composition, looks very much like Fig. 1 to the eye and is hence not presented. We obtain reasonable results with the short simulation. When we examine the regression coefficients in Table 2, we see

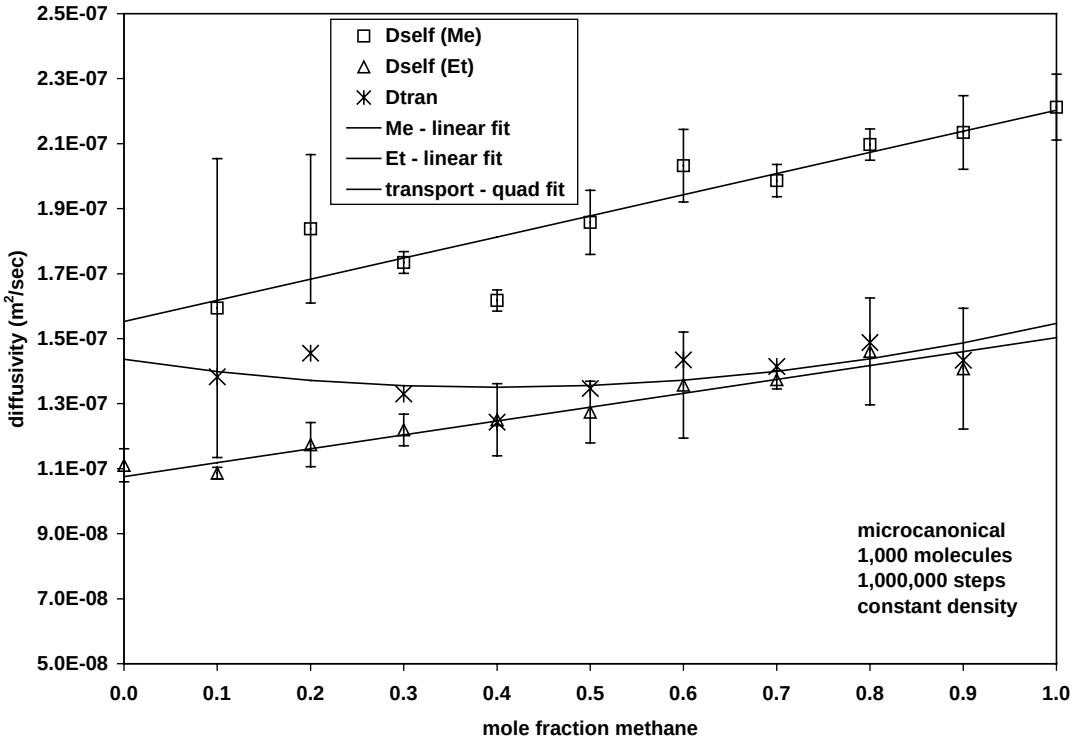

Fig. 3. Self-diffusivities and transport diffusivity for mixtures of methane and ethane as a function of composition at a temperature of 350 K and a density of 2.547×10^{-3} molecules/Å^3. These results come from the microcanonical ensemble using small system parameters of 10^3 molecules and 10^6 production steps. The polynomial fits are provided for statistical purposes only.

that all coefficients have standards deviations that overlap with the base case. Therefore, in practice, we could use the short simulation to obtain reliable self-diffusivities. In the present work, we continue to run the longer simulations of the base case because we are making special efforts to minimize noise in the data for the purposes of establishing the composition dependence of the transport diffusivity.

4.2. Diffusivity sensitivity to choice of ensemble

The choice of ensemble in which the system is simulated should not affect the value of the diffusivity. In this work, we are interested in establishing the dependence of the transport diffusivity on both (i) the composition and pressure holding temperature and density constant; and (ii) the composition and density holding temperature and pressure constant. The first task naturally requires simulation in the canonical ensemble. The second task naturally requires simulation in the isobaric–isothermal ensemble. Therefore, we wish to demonstrate and verify that the canonical and isobaric–isothermal ensembles yield the same results as those given by the microcanonical ensemble in Figs. 1 and 3 as well as Table 2.

The first step in implementing the canonical ensemble using the Melchionna reformulation of the Nosé–Hoover thermostat is to select a value of the temperature-controlling frequency, ν_T. In order to determine an appropriate value of ν_T, we performed canonical simulations (using base case parameters) for a 50/50 mixture of methane and ethane, where we varied the value of ν_T from 10^{-10} to $10^{-2}\,\text{fs}^{-1}$ in increments of one decade. We then plotted the mean values and standard deviations of the thermodynamic and transport properties as a function of ν_T, not shown here. Because we are simulating an equilibrium system, the properties were weak functions of ν_T, until we tried values larger than $10^{-2}\,\text{fs}^{-1}$, at which point our errors are due to instabilities in the Gear predictor-corrector because the thermostat is now acting on the same time scale as our integration time step. Based on this analysis, we selected $\nu_T = 10^{-5}\,\text{fs}^{-1}$, which allows for very gentle temperature control in a simulation of length 2×10^6 fs (as is our base case).

We need to repeat a comment regarding a nuance in the calculation of the diffusivity in the canonical ensemble. In the microcanonical ensemble, both energy and momentum are conserved. Because momentum is conserved, the center of mass of the system is stationary. Therefore, in a microcanonical ensemble the center-of-mass frame of reference coincides with the laboratory frame of reference. However, in the canonical ensemble, neither energy nor momentum is conserved for mixtures. (it is true that momentum is conserved for single component systems). Therefore, it is possible to observe a drift in the center of mass of the entire simulation volume using the canonical ensemble. Therefore, we calculated self-diffusivities using both Eqs. (1) and (19), so that we could obtain it relative to the laboratory frame-of-reference and the center-of-mass reference. For small systems, we observed a difference between the two diffusivities. For our base system, the error was less than 10^{-6}%, which is certainly negligible given the other uncertainties in the simulation. That being the case, in the simulations in the canonical and isobaric–isothermal ensembles, the laboratory frame-of-reference and the center-of-mass reference coincide.

The results of a series of canonical simulations for our base case simulation set as a function of composition duplicate the simulations shown in Figs. 1 and 3 and Table 2 and are hence not presented. The exception is that now we are using the canonical ensemble with $\nu_T = 10^{-5}\,\text{fs}^{-1}$. The average mean temperature of the eleven simulations was 350.01 K with an average standard deviation of 1.19 K. The canonical simulations duplicated the microcanonical results for the thermodynamic properties. For example, the average percent difference between the pressures for the two sets of simulations was 0.14%. The diffusivities generated from the canonical simulations are in quantitative agreement with the microcanonical simulations. To statistically justify this statement, we can compare the regression coefficients for the linear fits to the self-diffusivities and the quadratic fit to the transport diffusivity as shown in Table 2. The average difference between the coefficients for the different ensembles is 0.56%. The standard deviations of the coefficients for the self-diffusivities overlap. The coefficients for the transport diffusivity from the canonical simulations are not as good, but we believe that this variation is within the error of our procedure. This discrepancy could be reduced by running multiple simulations. However, the advantage of using the Darken equation to obtain transport diffusivities is that it requires only one simulation. If we lose this advantage, there is no reason to use the Darken equation in favor of a more rigorous approach.

We also verified that simulations in the isobaric–isothermal ensemble reproduce the results from the microcanonical and canonical ensembles. We specified the set pressure for each simulation in the isobaric–isothermal ensemble as the average pressure from the canonical ensemble. The density varies in these simulations. As was the case for the canonical ensemble, the first step in implementing the isobaric–isothermal ensemble using the Melchionna barostat is to select a value of the pressure-controlling frequency, ν_P. This selection was done in a manner analogous to the method used to determine ν_T. We simulated a 50/50 mixture of methane and ethane at the set temperature 350 K and the set pressure of 96.93 atm using 10^4 molecules and 10^6 time steps for values of $\log(\nu_P)$ ranging from 10^{-10} to $10^{-3}\,\text{fs}^{-1}$. Using the same selection criteria as was employed in the determination of ν_T, we chose a base value of $\nu_P = 10^{-5}\,\text{fs}^{-1}$. Neither energy nor momentum is conserved in the isobaric–isothermal ensemble. Therefore, it was again necessary to compute diffusivities corrected to the center-of-mass frame of reference. Again, we found no difference in the first eight digits (well beyond the accuracy of these simulations) of

the self-diffusivities in the laboratory and center-of-mass frames of reference.

The results of a series of isobaric–isothermal simulations for our base case simulation set as a function of composition duplicate the microcanonical simulations shown in Fig. 1 and the canonical simulations, except that now we are using the isobaric–isothermal ensemble with $\nu_T = 10^{-5}\,\mathrm{fs}^{-1}$ and $\nu_P = 10^{-5}\,\mathrm{fs}^{-1}$. The average mean temperature of the eleven simulations was 350.00 K with an average standard deviation of 1.21 K. The isobaric–isothermal simulations duplicated the microcanonical results for the thermodynamic properties. For example, the average percent difference between the pressures for the two sets of simulations was 0.06% and the average percent difference between the molar densities for the two sets of simulations was 0.14%. The diffusivities from the isobaric–isothermal simulations are in quantitative agreement with the microcanonical simulations. To statistically justify this statement, we can compare the regression coefficients for the linear fits to the self-diffusivities and the quadratic fit to the transport diffusivity as shown in Table 2. The agreement between coefficients for the self-diffusivity is excellent. The average difference between the coefficients for the different ensembles is 0.78%. The coefficients for the transport diffusivity from the isobaric–isothermal simulations are within the error bars of the microcanonical values.

At this point we have established that with (i) large systems; (ii) long simulations; (iii) carefully chosen temperature- and pressure-controlling frequencies; and (iv) the appropriate frame of reference of the self-diffusivity, that simulations in the microcanonical, canonical, and isobaric–isothermal ensembles can yield reproducible self-diffusivities and transport diffusivities. In the work that follows, we will use only one ensemble for each analysis, choosing the one that naturally applies. For example, when we establish the relationship between diffusivity and composition holding pressure and temperature constant we will use the isobaric–isothermal ensemble. However, when we establish the relationship between diffusivity and temperature holding composition and density constant we will use the canonical ensemble.

4.3. Diffusivity as a function of thermodynamic state

We can revisit Fig. 1, with the aim of explaining the relationship between diffusivity and composition when holding the density and temperature constant. It is clear from Fig. 2 that the pressure increases with increasing methane mole fraction. It may be counter-intuitive to think that the self-diffusivity of a material should increase with increasing pressure. However, this line of thinking assumes that with an increase in pressure, density increases. When dealing with a multicomponent mixture, this is not necessarily the case. In these simulations, the increase in pressure was due to the increase in methane mole fraction, as explained above. Since methane has a smaller mass than ethane, we can expect on the basis of kinetic theory (Eq. (6)) that it should diffuse faster.

In Fig. 4, we plot the predictions of kinetic theory for dilute gases, Eq. (8), and the average of the self-diffusivities from the microcanonical, canonical, and isobaric–isothermal ensembles. While the qualitative trends are captured, the results are quantitatively wrong. The root-mean-square error for Eq. (8) relative to the simulation results is 38% for methane and 35% for ethane. This error is not surprising, since we simulated a high-pressure fluid and Eq. (8) applies to dilute gases.

Using Eq. (12) in conjunction with a corresponding states chart, we were able to predict the self-diffusivities of methane and ethane for the states we simulated. Note, that the mean critical properties are used not only in Eq. (12) but also to calculate the reduced temperature and pressure required to use the corresponding-states plot. These predictions are shown in Fig. 5. The predictions are quantitatively accurate. The root-mean-square errors for Eq. (12) and a corresponding-states plot relative to the simulation results is 5.4% for methane and 2.9% for ethane.

We can now attempt to predict the transport diffusivity. We will make three different approximations. The first is to use our modified version of Eq. (13). The predictions of Eq. (13) are shown in Fig. 4. The predictions are quantitatively wrong, although they do seem to capture the correct qualitative trend. The root-mean-square error for Eq. (13) is 55%.

We use Eq. (15) and a corresponding-state chart to predict the transport diffusivity in Fig. 5. This prediction while quantitatively reasonable, predicts the wrong qualitative trend. The root-mean-square error for Eq. (15) is 14%. The prediction fails to capture the curvature of the transport diffusivity as a function of mole fraction.

A third prediction of the transport diffusivity is to use the self-diffusivities predicted by Eq. (12) and the corresponding states chart (plotted in Fig. 5) in the Darken equation, Eq. (3). We show this prediction in Fig. 5. The predictions are both qualitatively and quantitatively accurate. The root-mean-square error relative to the simulation results is 4.7%. We should be careful to remark that the accuracy of this last estimation of the transport diffusivity is not a vindication of the Darken equation, since the transport diffusivity calculated from both the simulation results and the theory used the Darken equation.

For the remainder of this work, we present simulation results using only one ensemble. Furthermore, we predict self-diffusivities using Eq. (12) and a corresponding states chart. We predict transport diffusivities using those self-diffusivities in the Darken equation.

We next performed a set of simulations in the isobaric–isothermal ensemble where we held the pressure and temperature constant at values of 96.76 atm and 350 K. We specified the composition and allowed the density to vary, in contrast to the previous simulations in which we specified the same molar density at all compositions and allowed

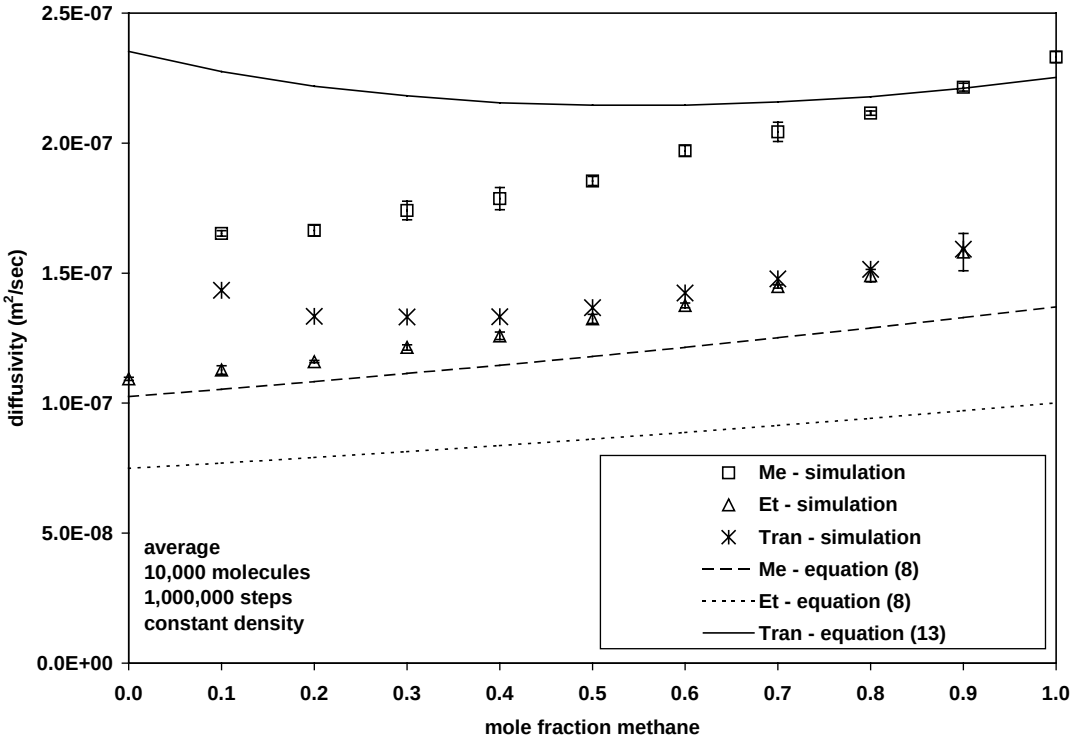

Fig. 4. Predictions of kinetic theory for the self-diffusivities and the prediction of an empirical correlation for the transport diffusivity. These simulation points are the average of those obtained from the base case simulations in the microcanonical, canonical and the isobaric–isothermal ensembles.

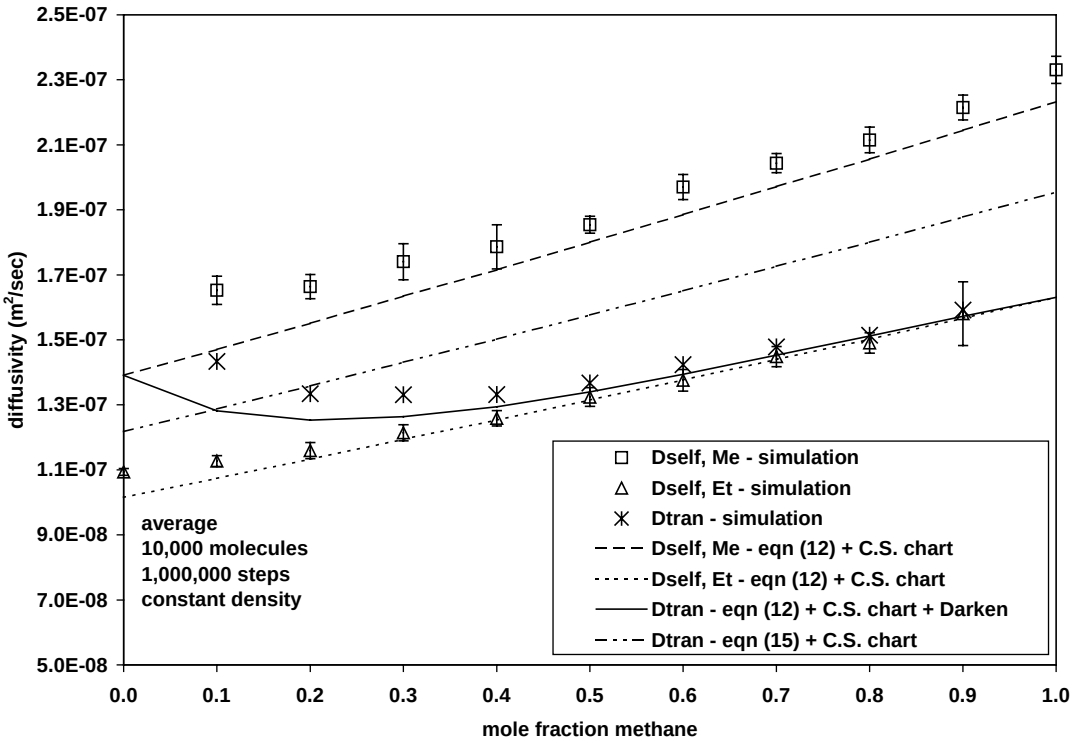

Fig. 5. Predictions of a corresponding states chart combined with kinetic theory. These simulation points are the average of those obtained from the base case simulations in the microcanonical, canonical and the isobaric–isothermal ensembles.

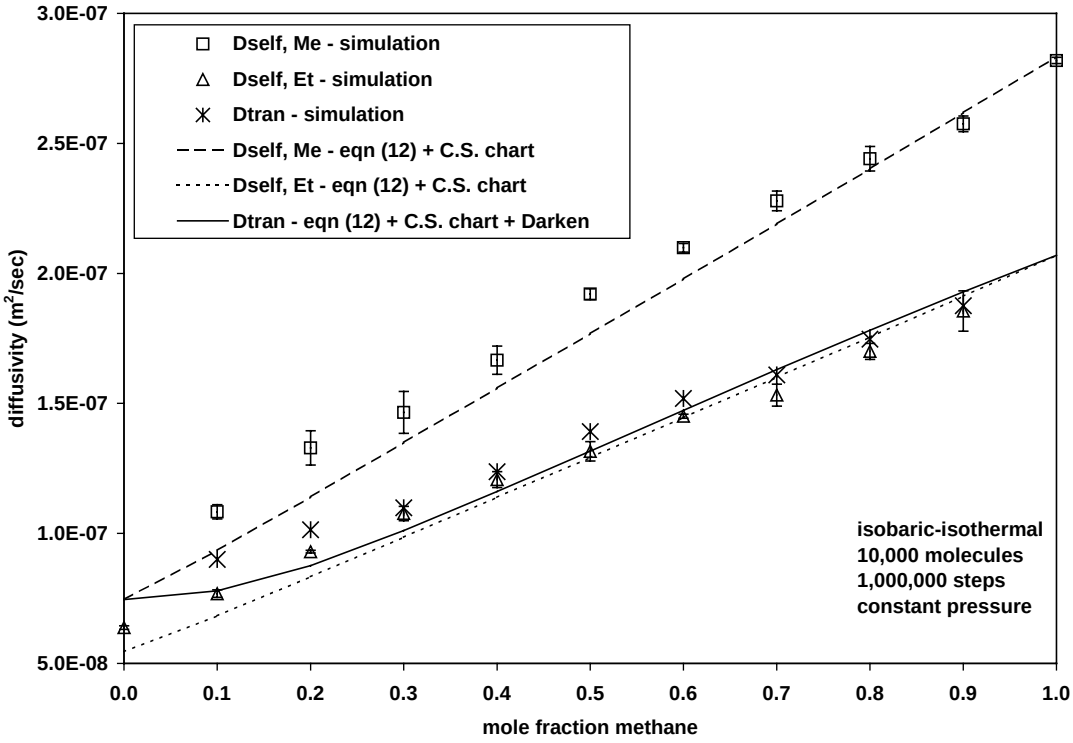

Fig. 6. Self-diffusivities and transport diffusivity for mixtures of methane and ethane as a function of composition at a temperature of 350 K and a pressure of 96.76 atm. These results come from the isobaric–isothermal ensemble using base case parameters of 10^4 molecules and 10^6 production steps. Also shown are the predictions of a corresponding states chart combined with kinetic theory.

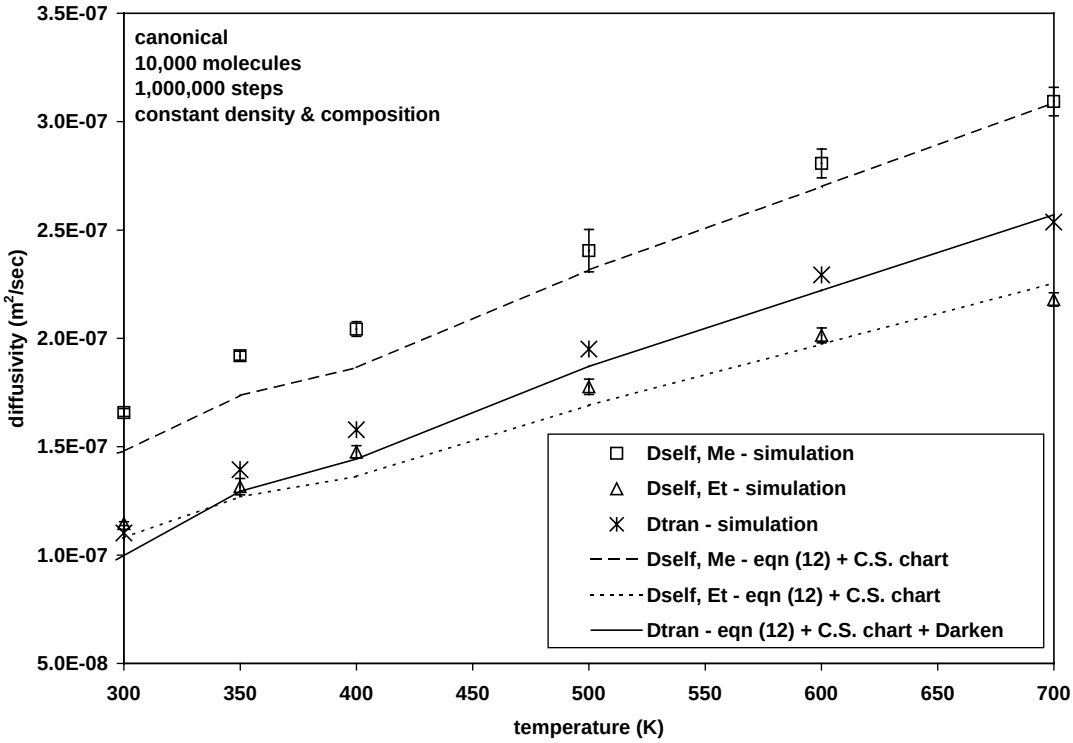

Fig. 7. Self-diffusivities and transport diffusivity for mixtures of methane and ethane as a function of temperature at a composition of 50/50 mol% methane/ethane and a density of 2.547×10^{-3} molecules/Å^3. These results come from the canonical ensemble using base case parameters of 10^4 molecules and 10^6 production steps. Also shown are the predictions of a corresponding states chart combined with kinetic theory.

the pressure to vary. In Fig. 6, we plot the self-diffusivity and transport-diffusivity as a function of mole fraction. The self-diffusivities increase with increasing mole fraction of methane. The cause of this increase is a decrease in the density. The molar density decreases with an increase in methane mole fraction, simply because at a given pressure and temperature, the Lennard–Jones attraction of methane is weaker than that of ethane. As a result of this decrease in molar density, the diffusivity increases. The predictions of Eq. (12) and the corresponding state chart are shown in Fig. 6. The predictions are both qualitatively accurate. The root-mean-square error for Eq. (12) and a corresponding-states plot relative to the simulation results is 7.7% for methane and 7.8% for ethane. The root-mean-square error for the prediction of the transport diffusivity using the predicted self-diffusivities and the Darken equation is 7.6%.

We also performed a set of simulations in the canonical ensemble where we held the composition and density constant at values of 50 mol% methane and 2.5474×10^{-3} molecules/Å^3. We specified the temperature over a range from 300 to 700 K and allowed the pressure to vary. In Fig. 7, we plot the self-diffusivity and transport-diffusivity as a function of temperature. As we increase the temperature holding the density and composition constant, the pressure increases. Intuitively, the increase in temperature should cause an increase in diffusivity, despite the increase in the pressure. The predictions from Eq. (12) and the corresponding states chart are not perfectly smooth, due to the inaccuracy involved in reading the corresponding states chart. However, this is a source of inaccuracy that the practicing engineer will face in predicting transport diffusivities. We see that our method of predicting self-diffusivities and transport diffusivities works across a broad range of temperatures. At higher temperatures, the fluid will continue to become more ideal with transport properties easier to predict.

We then performed a set of simulations in the isobaric–isothermal ensemble where we held the composition and pressure constant at values of 50 mol% methane and 96.76 atm. We specified the temperature over a range from 300 to 700 K and allowed the density to vary. In Fig. 8, we plot the self-diffusivity and transport-diffusivity as a function of temperature. As we increase the temperature holding the pressure and composition constant, the density decreases. Again, the increase in temperature should cause an increase in diffusivity. The decrease in density should also contribute to an increase in diffusivity. The predictions from Eq. (12) model the temperature dependence extremely well.

Finally, we performed a set of simulations in the isobaric–isothermal ensemble where we held the composition and temperature constant at values of 50% methane and 350 K. We specified the pressure over a broad range and allowed the density to vary. In Fig. 9, we plot the self-diffusivity and transport-diffusivity as a function of pressure. This figure is on a log–log scale, because the pressure range is so broad. The prediction of Eq. (12) and

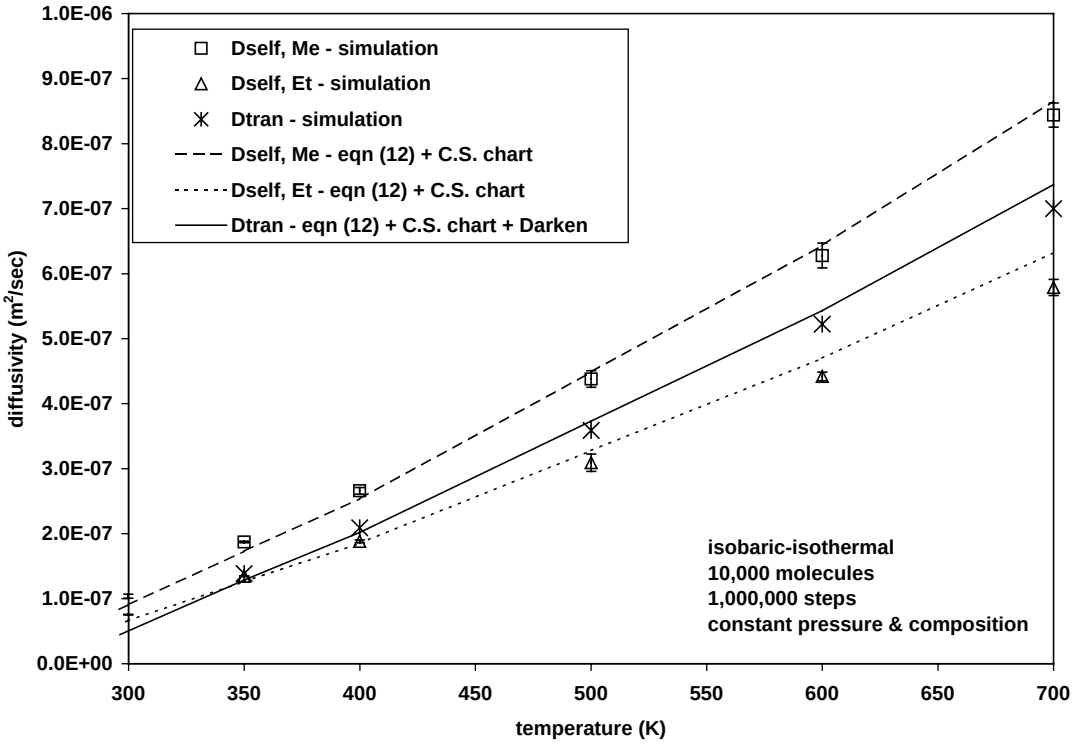

Fig. 8. Self-diffusivities and transport diffusivity for mixtures of methane and ethane as a function of temperature at a composition of 50/50 mol% methane/ethane and a pressure of 96.76 atm. These results come from the isobaric–isothermal ensemble using base case parameters of 10^4 molecules and 10^6 production steps. Also shown are the predictions of a corresponding states chart combined with kinetic theory.

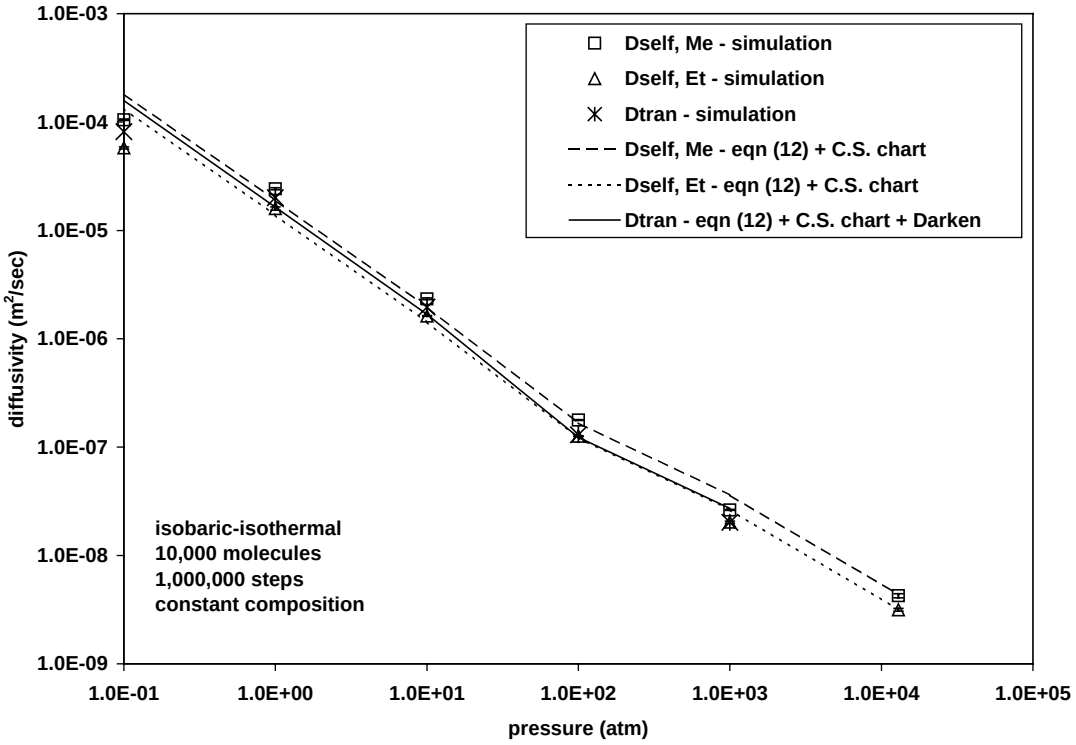

Fig. 9. Self-diffusivities and transport diffusivity for mixtures of methane and ethane as a function of pressure at a composition of 50/50 mol% methane/ethane and a temperature of 350 K. These results come from the isobaric–isothermal ensemble using base case parameters of 10^4 molecules and 10^6 production steps. Also shown are the predictions of a corresponding states chart combined with kinetic theory.

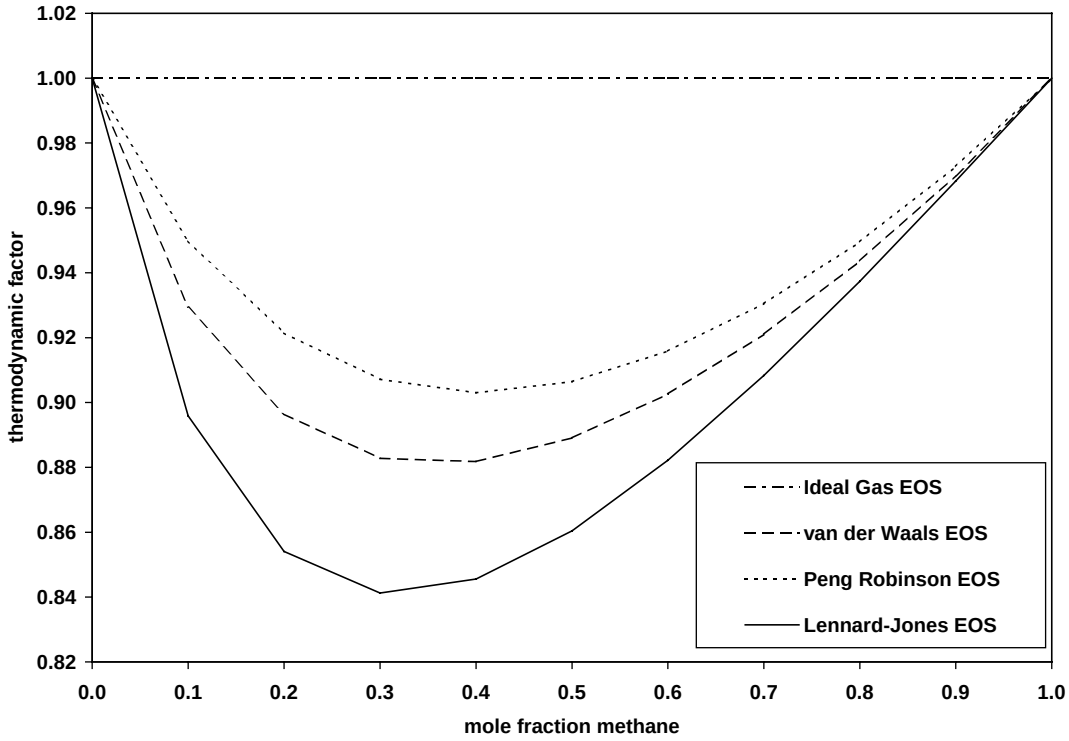

Fig. 10. The thermodynamic factor in the Darken equation as a function of equation of state at a temperature of 350 K and a density of 2.547×10^{-3} molecules/Å^3.

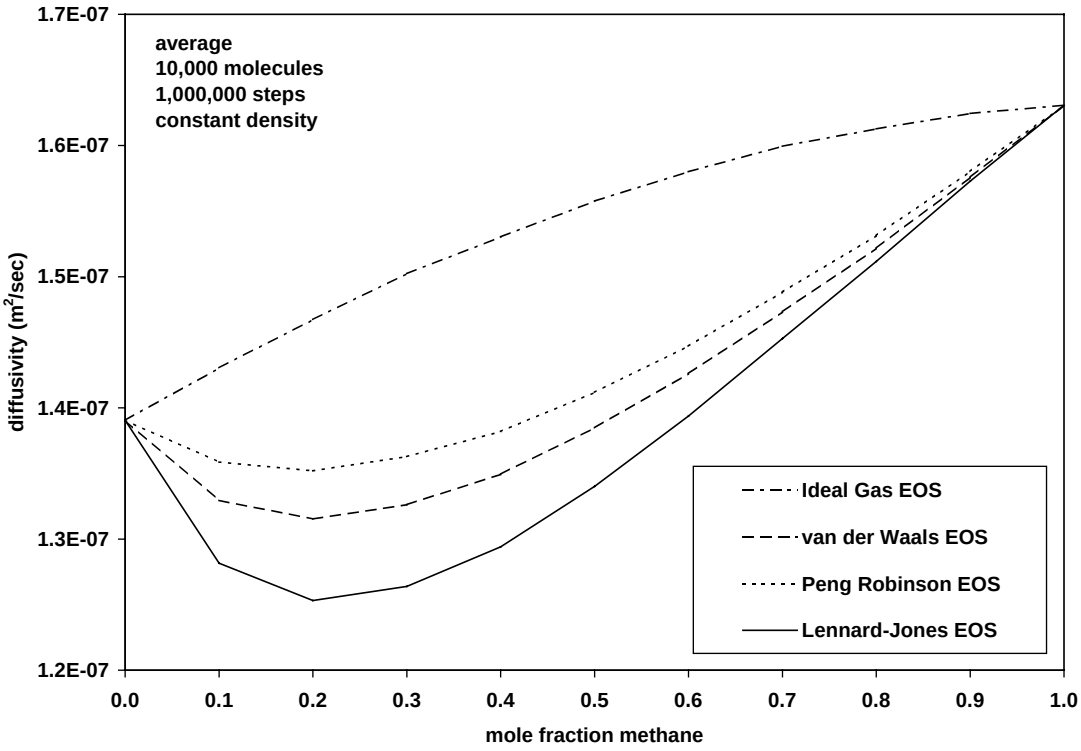

Fig. 11. The transport diffusivity as a function of equation of state at a temperature of 350 K and a density of 2.547×10^{-3} molecules/Å^3. The self-diffusivities used to generate this plot are the average of those obtained from the base case simulations in the microcanonical, canonical and the isobaric–isothermal ensembles.

the corresponding states chart does not extend through all of the simulation data, due to the fact that the chart only applies up to a reduced pressure of 10. Once the pressure is greater than 10 times the critical pressure, the charts cannot be used to compare with the simulation data.

4.4. Transport diffusivity sensitivity to equation of state

All of the transport diffusivities reported thus far have been calculated using Darken's equation. We evaluated the thermodynamic partial derivative appearing in the Darken equation using the Lennard–Jones equation of state. In Figs. 10 and 11, we examine the effect of the equation of state on the transport diffusivity. We choose as our self-diffusivities that feed into the Darken equation the average of the self-diffusivities from the microcanonical, canonical, and isobaric–isothermal ensembles. In these plots, the temperature and the density are fixed. The pressure varies as was shown in Fig. 2. In Fig. 10, we plot the thermodynamic factor in the Darken equation for four different equations of state: the ideal gas EOS, the van der Waals EOS, the Peng–Robinson EOS, and the Lennard–Jones EOS. We see that the equation of state does play a significant role in determining the thermodynamic factor of a high pressure mixture. In Fig. 11, we observe the effect that the choice of equation of state has on the transport diffusivity. The concavity of the transport diffusivity with respect to composition is a function of the equation of state. With the ideal gas, where the thermodynamic factor is unity, the second derivative of the transport diffusivity with respect to mole fraction is negative. However, because the other three equations of state have thermodynamic factors, which deviate sufficiently below unity, they cause a net positive concavity.

5. Conclusions

In this work, we have conducted extensive molecular dynamics simulations of a mixture of methane and ethane at high pressures. We have used the simulations, in conjunction with the Darken equation and the Lennard–Jones equation of state, to determine the transport diffusivity and its functional dependence on composition, density, pressure, and temperature. While the Darken equation is an approximate relation and while the use of an equation of state adds a second approximation, this method has the advantage that it can deliver a statistically reliable transport diffusivity with a single equilibrium simulation. We have found that by using mixing rules for the critical properties, one can use existing correlations and corresponding states charts to predict the self-diffusivities and transport diffusivities to within less than 10%.

We have demonstrated that careful simulations in the microcanonical, canonical, and isobaric–isothermal ensemble yield the same thermodynamic and transport properties. We have also demonstrated that equilibrium simulations with

more molecules than is typically used are required in order to obtain a statistically significant composition dependence of the transport diffusivity.

It is our intention to present follow up of this investigation with a discussion of the composition dependence of the transport diffusivity obtained from many simulations yielding phenomenological coefficients. At that point, we will be able to comment on the validity of the Darken equation for mixtures of small, nonpolar molecules at high pressure.

Acknowledgements

These simulations were performed on four different machines. A two-processor workstation was made available by the Department of Chemical Engineering at the University of Tennesee. A 16-processor cluster was made available by the University of Tennessee Technology Fee and the College of Engineering. Access to two machines, a 184-node IBM RS/6000 SP and a 64-node Compaq AlphaServer at Oak Ridge National Laboratory was made possible through the UT/ORNL Joint Institute of Computational Science. P.A. would like to acknowledge support from the UT Engineering Fundamentals Division.

References

[1] S. Chapman, T.G. Cowling, The Mathematical Theory of Nonuniform Gases, second ed., Cambridge University Press, Cambridge, 1952); J.O. Hirschfelder, C.F. Curtiss, R.B. Bird, Molecular Theory of Gases and Liquids, Wiley, New York, 1954.
[2] R.C. Reid, T.K. Sherwood, The Properties of Gases and Liquids. Their Estimation and Correlation, second ed., McGraw-Hill, New York, 1966.
[3] R.B. Bird, W.E. Stewart, E.N. Lightfoot, Transport Phenomena, second ed., Wiley, New York, 2002.
[4] M.P. Allen, D.J. Tildesley, Computer Simulation of Liquids, Oxford Science Publications Oxford, 1987.
[5] J.M. Haile, Molecular Dynamics Simulation, Wiley, New York, 1992.
[6] D. Frenkel, B. Smit, Understanding Molecular Simulation, Academic Press, San Diego, 1996.
[7] G.S. Heffelfinger, F. van Swol, J. Chem. Phys. 100 (10) (1994) 7548.
[8] E.J. Maginn, A.T. Bell, D.N. Theodorou, J. Phys. Chem. 97 (16) (1993) 4173.
[9] G. Arya, H.-C. Chang, E.J. Maginn, J. Chem. Phys. 115 (17) (2001) 8112.
[10] L.S. Darken, Trans. Am. Inst. Mining Metall. Eng. 175 (1948) 184.
[11] P.C. Carman, J. Phys. Chem. 71 (8) (1967) 2565.
[12] P.C. Carman, J. Phys. Chem. 72 (5) (1968) 1707; P.C. Carman, J. Phys. Chem. 72 (5) (1968) 1713; R.K. Ghai, H. Ertl, F.A.L. Dullien, AIChE J. 19 (5) (1973) 881; R.K. Ghai, H. Ertl, F.A.L. Dullien, AIChE J. 20 (1) (1974) 1; D.W. McCall, D.C. Douglass, J. Phys. Chem. 71 (4) (1967) 987; A.L. van Geet, A.W. Adamson, J. Phys. Chem. 68 (2) (1964) 238.
[13] M. Helbaek, B. Hafskjold, D.K. Dysthe, G.H. Sorland, J. Chem. Eng. Data 41 (3) (1996) 598; H. Higashi, Y. Iwai, Y. Nakamura, S. Yamamoto, Y. Arai, Fluid Phase Equilib. 166 (1999) 101.
[14] D.N. Theodorou, R.Q. Snurr, A.T. Bell, in: G. Alberti, T. Bein (Eds.), Comprehensive Supramolecular Chemistry, vol. 7, Permagon Press, New York, 1996, p. 507.; M.J. Sanborn, R.Q. Snurr, AIChE J. 47 (9) (2001) 2032.
[15] M.J. Sanborn, R.Q. Snurr, Separation Purif. Technol. 20 (2000) 1.
[16] D.L. Jolly, R.J. Bearman, Mol. Phys. 41 (1) (1980) 137.
[17] M. Schoen, C. Hoheisel, Mol. Phys. 52 (5) (1984) 1029; M. Schoen, C. Hoheisel, Mol. Phys. 52 (1) (1984) 33; F.O. Raineri, H.L. Friedman, Mol. Phys. 70 (2) (1990) 209; D. MacGowan, Mol. Phys. 59 (5) (1986) 1017; P.J. Gardner, D.M. Heyes, S.R. Preston, Mol. Phys. 73 (1) (1991) 141; J.M. Stoker, R.L. Rowley, J. Chem. Phys. 3670 (6) (1989) 3670.
[18] S.M. Ali, A. Samanta, S.K. Ghosh, J. Chem. Phys. 114 (23) (2001) 10419.
[19] B. Widom, J. Phys. Chem. 86 (1982) 869.
[20] J.J. Nicolas, K.E. Gubbins, W.B. Streett, D.J. Tildesley, Mol. Phys. 37 (5) (1979) 1429.
[21] J.C. Slattery, R.B. Bird, AIChE J. 4 (1958) 137.
[22] W.G. Hoover, Phys. Rev. A 31 (3) (1985) 1695.
[23] S. Melchionna, G. Ciccotti, B.L. Holian, Mol. Phys. 78 (3) (1993) 533.
[24] S. Nosé, Mol. Phys. 52 (2) (1984) 255.
[25] H.J.C. Berendsen, J.P.M. Postma, W.F. van Gunsteren, A. DiNola, J.R. Haak, J. Chem. Phys. 81 (8) (1984) 3684.
[26] S. Nosé, M.L. Klein, Mol. Phys. 50 (5) (1983) 1055.
[27] S.I. Sandler, Chemical and Engineering Thermodynamics, second ed., John Wiley, New York, 1989.